International Journal of
Molecular Sciences

MDPI

Article

Chronically Radiation-Exposed Survivor Glioblastoma Cells Display Poor Response to Chk1 Inhibition under Hypoxia

Nareg Pinarbasi-Degirmenci [1,2], Ilknur Sur-Erdem [1,2,*], Vuslat Akcay [1,2], Yasemin Bolukbasi [3,4], Ugur Selek [3,4], Ihsan Solaroglu [2,5,6] and Tugba Bagci-Onder [1,2,*]

1 Brain Cancer Research and Therapy Laboratory, Koç University School of Medicine, Istanbul 34450, Turkey; npinarbasi18@ku.edu.tr (N.P.-D.); vuslat.akcay@dkfz-heidelberg.de (V.A.)
2 Research Center for Translational Medicine, Koç University, Istanbul 34450, Turkey; isolaroglu@ku.edu.tr
3 Department of Radiation Oncology, Koç University School of Medicine, Istanbul 34010, Turkey; ybolukbasi@kuh.ku.edu.tr (Y.B.); ugurselek@yahoo.com (U.S.)
4 Division of Radiation Oncology, The University of Texas MD Anderson Cancer Center, Houston, TX 77030, USA
5 Department of Neurosurgery, Koç University School of Medicine, Istanbul 34010, Turkey
6 Department of Basic Sciences, Loma Linda University, Loma Linda, CA 92354, USA
* Correspondence: ilknursur@gmail.com (I.S.-E.); tuonder@ku.edu.tr (T.B.-O.)

Abstract: Glioblastoma is the most malignant primary brain tumor, and a cornerstone in its treatment is radiotherapy. However, tumor cells surviving after irradiation indicates treatment failure; therefore, better understanding of the mechanisms regulating radiotherapy response is of utmost importance. In this study, we generated clinically relevant irradiation-exposed models by applying fractionated radiotherapy over a long time and selecting irradiation-survivor (IR-Surv) glioblastoma cells. We examined the transcriptomic alterations, cell cycle and growth rate changes and responses to secondary radiotherapy and DNA damage response (DDR) modulators. Accordingly, IR-Surv cells exhibited slower growth and partly retained their ability to resist secondary irradiation. Concomitantly, IR-Surv cells upregulated the expression of DDR-related genes, such as *CHK1*, *ATM*, *ATR*, and *MGMT*, and had better DNA repair capacity. IR-Surv cells displayed downregulation of hypoxic signature and lower induction of hypoxia target genes, compared to naïve glioblastoma cells. Moreover, Chk1 inhibition alone or in combination with irradiation significantly reduced cell viability in both naïve and IR-Surv cells. However, IR-Surv cells' response to Chk1 inhibition markedly decreased under hypoxic conditions. Taken together, we demonstrate the utility of combining DDR inhibitors and irradiation as a successful approach for both naïve and IR-Surv glioblastoma cells as long as cells are refrained from hypoxic conditions.

Keywords: glioblastoma; radiotherapy; radioresistance; hypoxia; DNA damage response; Chk1

Citation: Pinarbasi-Degirmenci, N.; Sur-Erdem, I.; Akcay, V.; Bolukbasi, Y.; Selek, U.; Solaroglu, I.; Bagci-Onder, T. Chronically Radiation-Exposed Survivor Glioblastoma Cells Display Poor Response to Chk1 Inhibition under Hypoxia. *Int. J. Mol. Sci.* **2022**, *23*, 7051. https://doi.org/10.3390/ijms23137051

Academic Editors: Jaroslaw MacIaczyk, Hugo Guerrero-Cazares and Amit Sharma

Received: 17 April 2022
Accepted: 10 June 2022
Published: 24 June 2022

1. Introduction

Glioblastoma remains a significant health problem with being an incurable malignant brain tumor in adults [1]. The standard of treatment for patients diagnosed with glioblastoma has long entailed tumor resection, followed by chemotherapy and radiotherapy as described in the landmark European Organization for Research and Treatment of Cancer (EORTC) Brain Tumor and Radiotherapy Group and the National Cancer Institute of Canada [2,3]. Recent genomic and molecular studies have shown that glioblastoma is the most heterogeneous disease among all cancer types and is composed of several cell populations with multiple genotypic origins [4]. Despite the advances in our understanding of glioblastoma genetics, cell-of-origin, or tumor heterogeneity, the survival rates have remained unchanged during the last decade.

Ionizing radiation (IR)-based radiotherapy is a gold therapeutic cornerstone for glioblastoma patients. It is applied as a fractionated clinical regimen, by administering

patients 2 Gy of IR over 5 days/week reaching a total of 60 Gy at the end of 6 weeks. However, despite IR and concomitantly applied chemotherapy with Temozolomide, a DNA alkylating agent, tumor recurrence is observed in majority of the patients. One of the mechanisms behind therapeutic failure is considered to be inherent or acquired therapy resistance of glioblastoma cells. The tumor cells that are radioresistant cannot be efficiently eradicated after a full dose of IR treatment suggesting that tumor cells develop adaptations to the applied therapies by undergoing genetic or epigenetic changes [5,6]. Repopulation by IR-exposed surviving glioblastoma cells during fractionated IR is among the main reasons for radiotherapy-resistant tumor recurrence [7]. To overcome this problem, several approaches for radiosensitization have been investigated, yet none of them has translated into the clinic to improve the radiosensitivity in glioblastoma patients so far [8]. Although different glioblastoma cell lines have been examined in this context, where they were exposed to short-term and low doses of IR, the behavior of glioblastoma cells after long-term and high-dose radiation (total 60 Gy) remains largely unknown [9–13]. Most pre-clinical studies that interrogated the low-dose IR response of glioblastoma cell lines have shown that the radiosensitization effect is achieved by mainly targeting DNA damage repair pathways, tumor microenvironment, and cancer stem cells, but there are conflicting results with respect to obtaining radiation-persistent models in those studies [14,15]. Currently, there are no effective therapies to target long-term–IR-exposed survivor (IR-Surv) cells.

Radiotherapy induces damage to the genetic material of the cell and affects numerous vital cellular mechanisms that may trigger radioresistance with persistent or irreparable DNA damage, activated DNA damage response (DDR), irreversible cell cycle arrest, and oncogene activation, besides several unknown reasons [16–18]. Furthermore, metabolic changes occur in response to IR treatment, by stimulating oxidative stress and hypoxic mechanisms. Hypoxia Inducible Factor 1 (HIF-1) stabilization or activation by IR triggers protective processes by regulating downstream target genes that can induce immunosuppressive and antiapoptotic responses [19]. Several studies reported the improvement of radiosensitivity by blocking DDR and hypoxia pathways [20,21]. Although targeting such pathways for glioblastoma therapy has shown promise in animal models, none has so far worked in clinical practice and improved patient survival [22,23]. Therefore, a better understanding of IR response in clinically relevant experimental cell models are needed to mimic radiobiological characteristics of tumors after standard clinically applied therapeutic regimens. Moreover, growing evidence suggests the host immunity and inflammation as two conditions impacting glioblastoma progression, which clinically stratifies patients into two significant outcome groups following the same radiochemotherapy protocols, pointing out the importance of tumor stroma and microenvironment in addition to tumor characteristics [24–28]. As radiotherapy targets not only the tumor but also the adjacent healthy brain tissue, the inflammation and hypoxic changes in stroma and its relationship with glioblastoma require further experimental modeling to resolve related clinical discrepancy.

In this study, we established human IR-Surv glioblastoma cell models in vitro by exposing cells to 40–60 Gy of fractionated radiotherapy. Using established and patient-derived cell lines, we selected radiation survivor cells and characterized the phenotypic and transcriptomic alterations in these cells. We demonstrated that DDR and hypoxia pathways have undergone major adaptations in IR-Surv cells in favor of improved DNA repair capacity. We showed that targeting these pathways using chemical inhibitors or switching oxygen conditions along with IR may serve as key therapeutic approaches for radiosensitization of IR-Surv cells and may be applied in the clinic to target recurrent tumors.

2. Results

2.1. Generation of Radiation Survivor (IR-Surv) Glioblastoma Cell Populations

To mimic the standardized radiotherapy protocol used in the clinic and generate clinically relevant irradiation-exposed cell populations, we used three established (U373, T98G, LN229) and one primary (KUGBM8) cell line and irradiated them to a total dose of 40–60 Gy, fractionated by 2 Gy five times a week. Parental cell lines were also passaged with

irradiated samples to establish age-matched controls (Figure 1A). LN229 and T98G cells could survive until a total dose of 30 Gy and KUGBM8 cells until 40 Gy. Cell populations that survived long-term IR exposure were named as IR Survivor (IR-Surv) cells. Since U373$^{60\ Gy}$ and KUGBM8$^{40\ Gy}$ IR-Surv cells persisted longer under high exposure to IR compared to other cell lines, we mainly focused on the characterization of these and their parental pairs.

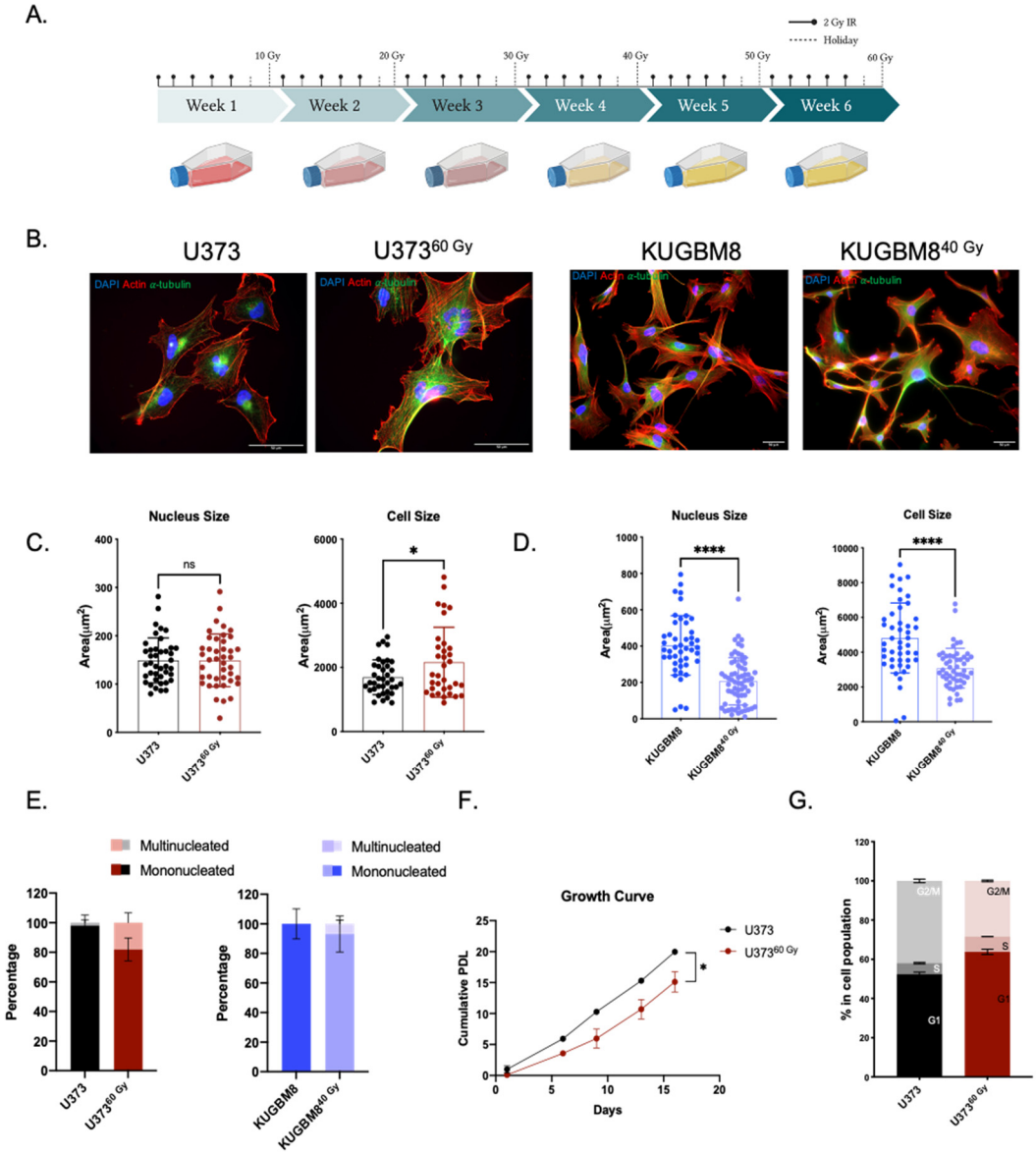

Figure 1. Generation of radiation survivor cell populations. (**A**) Experimental setup for generation of radiation survivor (IR-Surv) cell populations (generated by Biorender.com). (**B**) Immunofluorescent staining for U373 and KUGBM8 naïve and IR-Surv populations. (DAPI: blue, Actin: red, α-tubulin: Green, scale bar: 50 μm). (**C**,**D**) Comparison of nuclei and cell sizes between naïve and IR-Surv cells (U373-U373$^{60\ Gy}$ $n = 55$, KUGBM8-KUGBM8$^{40\ Gy}$ $n = 78$). (**E**) Multinucleated cell ratios upon IR-exposure of U373 and U373$^{60\ Gy}$ cells. (**F**). Proliferation rates of U373 and U373$^{60\ Gy}$ cells. (**G**) Cell cycle distributions of U373 and U373$^{60\ Gy}$ cells for *p*-values, *, and **** denote $p < 0.05$, $p < 0.0001$, respectively, two-tailed Student's *t*-test, ns denote not significant.

The morphological analysis revealed that irradiation caused a significant increase in cell size in U373$^{60\ Gy}$ cells without affecting nucleus size. Specifically, average cell size was 1693 ± 89 μm^2 in U373 cells and 2734 ± 473 μm^2 in U373$^{60\ Gy}$ cells. Nucleus sizes

were comparable in U373 and U373$^{60\ Gy}$ cells, as 149 ± 8 and 165 ± 12 μm^2, respectively (Figure 1B,C). Compared to their parental cells, both nucleus and cell size decreased in KUGBM8$^{40\ Gy}$ cells. While cell sizes were 6171 ± 1009 and 4239 ± 912 μm^2, nucleus sizes were 502 ± 63 and 389 ± 73 μm^2 in KUGBM8 and KUGBM8$^{40\ Gy}$ cells, respectively (Figure 1D). The percentage of multinucleated cells in the population increased in U373$^{60\ Gy}$ and KUGBM8$^{40\ Gy}$ compared to their parental pairs (Figure 1E), consistent with the previous reports on HepG2 cells [29]. We have not observed any significant alteration in the morphology of IR-exposed T98G and LN229 cells (Supplementary Figure S1C). Long-term IR exposure also affected proliferation rates; the proliferation rate of U373$^{60\ Gy}$ cells was slower than U373 (Figure 1F). However, we observed a slightly increased proliferation rate in KUGBM8$^{40\ Gy}$ cells (Supplementary Figure S1A). In addition, there were significant differences in the cell cycle distribution of IR-Surv cells and their parental pairs. The percent number of U373$^{60\ Gy}$ cells in the G1 phase of the cell cycle was higher than its parental pair (Figure 1G), but we did not observe a significant change in the cell cycle distribution of KUGBM8 cells (Supplementary Figure S1B).

To investigate whether selected IR-Surv cells maintain their persistent phenotype with secondary irradiation, we tested the viability of U373$^{60\ Gy}$ and KUGBM8$^{40\ Gy}$ cells in response to varying amounts of single-dose irradiation with clonogenic assays, which can be considered as a gold standard to assess the long-term effects of chemoradiation studies [30]. To this end, cells were exposed to 2, 4, 6, and 8 Gy of a single dose of irradiation, and colony-forming ability was measured after 14 days (Figure 2A). Accordingly, U373$^{60\ Gy}$ cells exhibited less response to radiation treatment and better colony-forming abilities than their parental pairs after 4, 6, and 8 Gy treatments (Figure 2B). In contrast, we did not observe any significant difference in colony-forming abilities of KUGBM8$^{40\ Gy}$ cells (Figure 2B, Supplementary Figure S1D). We also examined whether there was any cross-resistance of IR-Surv cells to Temozolomide (TMZ), the clinically applied chemotherapeutic for glioblastoma [2]. We treated naïve and IR-Surv cells with increasing doses of TMZ and examined different responses of IR-Surv cells. Accordingly, U373$^{60\ Gy}$ cells had a higher IC50 value of TMZ than its parental pair and displayed a TMZ-resistant behavior (IC_{50}U373 = 18.81 μM, IC_{50}U373$^{60\ Gy}$ = 80.75 μM) (Figure 2D). However, KUGBM8$^{40\ Gy}$ cells displayed a better response to TMZ than their parental pair. For further elucidation of secondary therapy response, we combined single-dose 4 Gy IR with high-dose (125 μM) TMZ. Similar to previous findings, U373$^{60\ Gy}$ cells had a higher tolerance to TMZ + IR combination, whereas KUGBM8$^{40\ Gy}$ cells were more sensitive (Figure 2E). There was no observed difference in the TMZ response of IR-Surv T98G or LN1229 cells (Supplementary Figure S1E). Together, we generated clinically relevant cell line models of IR-surviving cells, one of which was derived from a well-known established cell line and the other one from a primary cell line. Despite their few differences, both IR-Surv cell lines displayed refractory behavior to secondary irradiation, mimicking the radioresistance observed in clinical settings.

2.2. Transcriptomics Analyses Reveal Changes in DNA Damage Response and Hypoxia Pathways in IR-Surv Cells

To understand global transcriptomic changes related to IR exposure and survival from it, RNA sequencing was performed on naïve and IR-Surv U373 and KUGBM8 cell populations. Replicates from each group were clustered together in a hierarchical clustering map and Principal Component Analysis (PCA) revealed good separation of U373, KUGBM8, and their IR-Surv subpopulations from each other (Supplementary Figure S2A,B). A total of 1346 genes were differentially expressed between U373 and U373$^{60\ Gy}$ cells; 803 of the genes were downregulated, and 543 of the genes were upregulated. These numbers were even higher between KUGBM8 and KUGBM8$^{40\ Gy}$ cells; 3153 genes were downregulated, and 2141 genes were upregulated (Figure 3A). In U373 IR-Surv cells, the top 10 upregulated and downregulated genes with the highest log2fold change with significance included *GDA*, *CLEC1A*, *FOXF1*, *RTN1*, *STEAP2*, *PDE10A*, *HGF*, *ADGRL2*, *HTR1F*, and *FMO3*;

and *IL21R*, *DPPA4*, *PLAC8*, *KCNG1*, *SLAMF9*, *SLCO4A1-AS1*, *PAGE2*, *NELL1*, *PEG3*, and *NELL2*, respectively. In KUGBM8 IR-Surv cells, the top 10 upregulated genes were *BTC*, *NPPA-AS1*, *DAB1*, *GAL*, *SERPINB2*, *TH*, *CYP4F11*, *PARP8*, *SLC4A1*, and *RADX*; and top 10 downregulated genes were *WNT6*, *CXCL13*, *FMOD*, *FGF21*, *ATP2A1*, *TMEM178A*, *DIPK1C*, *BPIFA2*, *PRTN3*, and *C1QL4* (Supplementary Figure S2C).

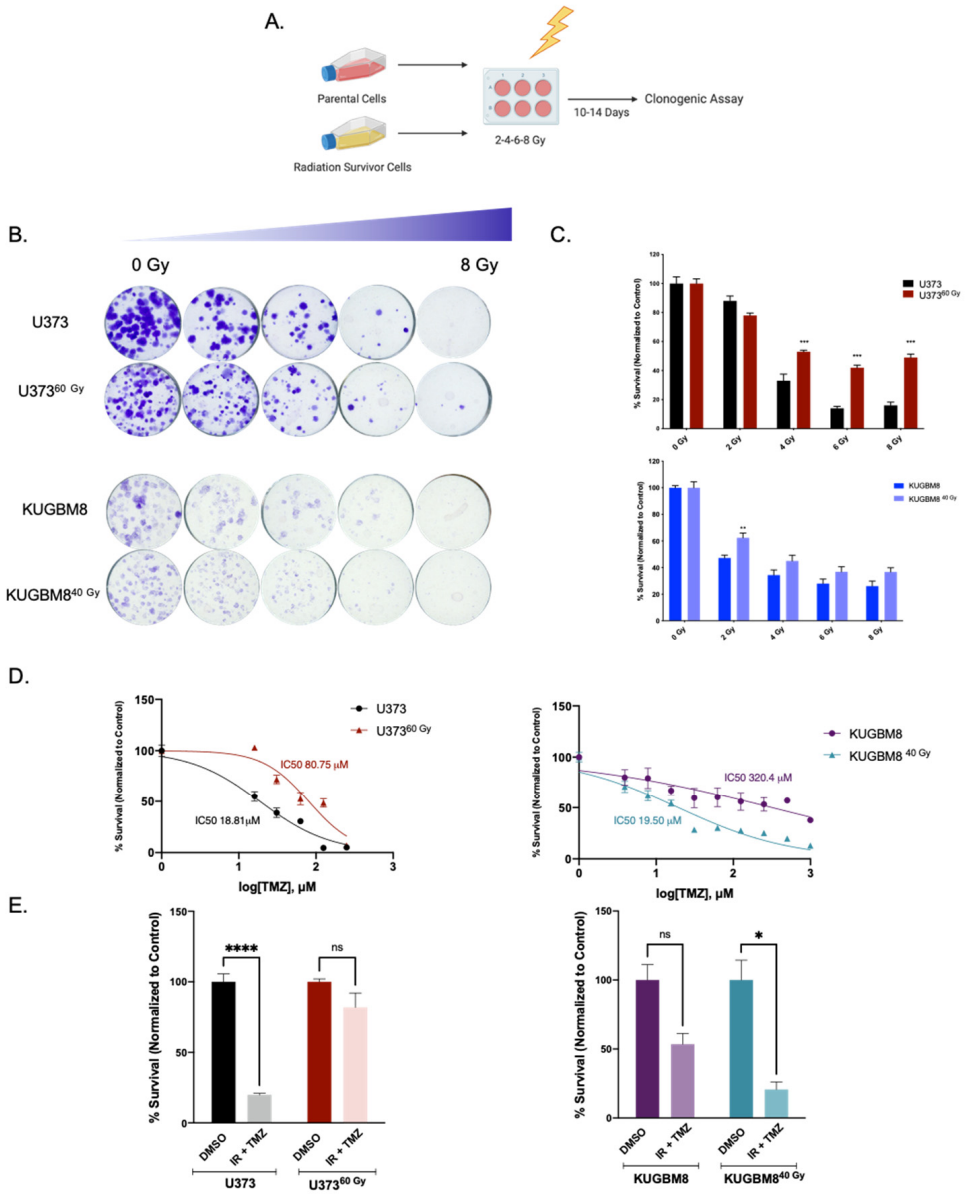

Figure 2. Effect of secondary IR treatment varies among different IR-Surv cells. (**A**) Schematic representation of experimental set up to test the effects of secondary ionizing radiation exposure (generated by Biorender.com). (**B**) Representative images of clonogenic assay of U373-U373$^{60\ Gy}$ and KUGBM8-KUGBM8$^{40\ Gy}$ cells upon single treatment with increasing doses of IR. (**C**) Quantification of colony numbers of naïve and IR-Surv U373 and KUGBM8 cells. (**D**) Dose-response curves of naïve and IR-Surv U373 and KUGBM8 cells upon TMZ treatment for 2 days. (**E**) Cell viabilities of cells 7 days after TMZ and IR combination treatment. (ns denote not significant, for *p*-values, *, **, ***, and **** denote $p < 0.05$, $p < 0.01$, $p < 0.001$, and $p < 0.0001$, respectively, two-way ANOVA).

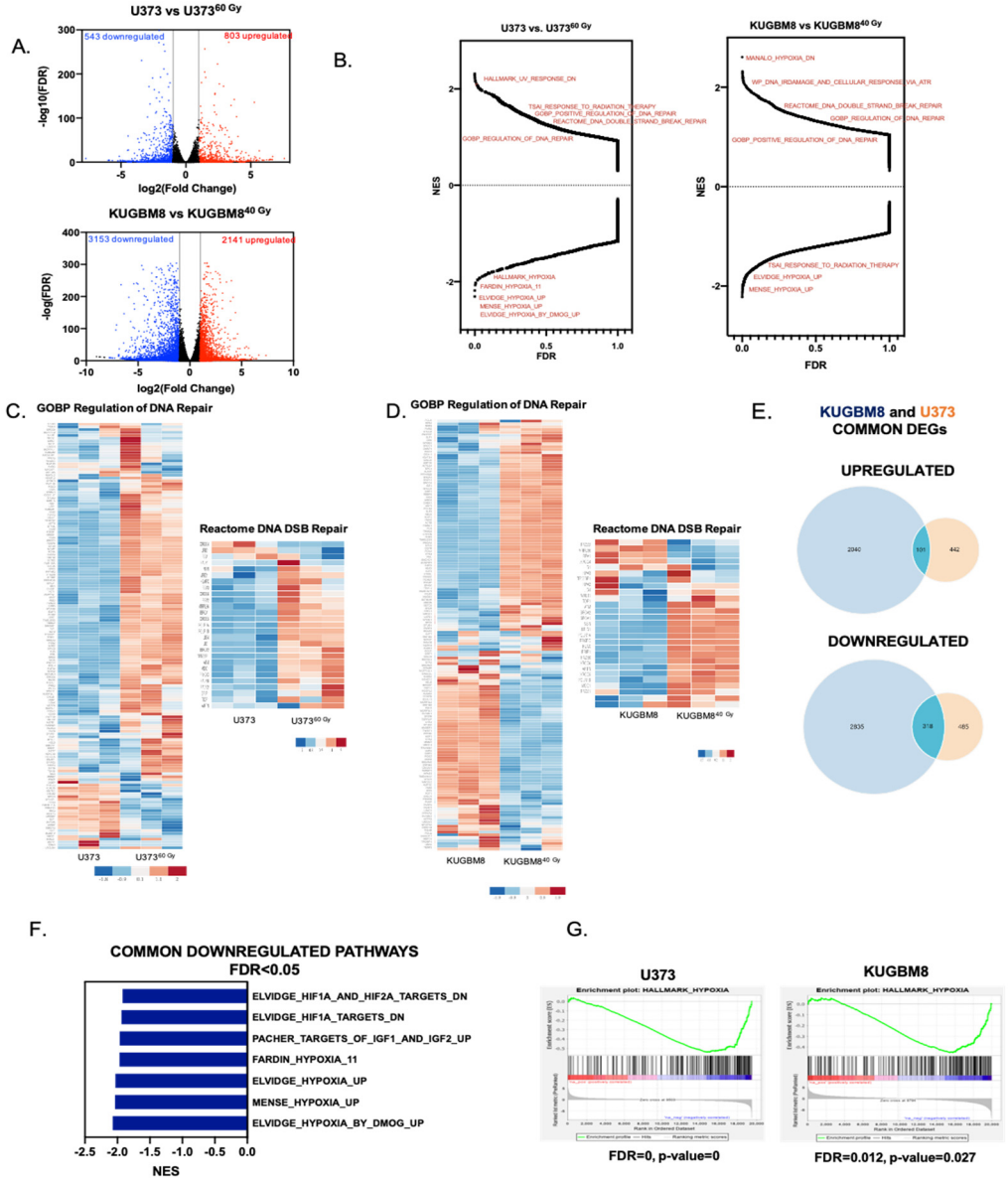

Figure 3. Transcriptomic alterations in IR-Surv cell populations. (**A**) Volcano plot showing the upregulated (red) and downregulated (blue) genes in IR-Surv U373 and KUGBM8 cells (Log2fold change > 1 and FDR < 0.05) (**B**) Gene Set Enrichment Analysis (GSEA) plots of U373 and KUGBM8 cells showing the distribution of all available gene sets. (**C**,**D**) Differential expression heat map of GOBP Regulation of DNA Repair and Reactome DNA DSB Repair gene sets for U373 and KUGBM8 cells. Heat map showing z-score of log2 transformed gene expression of selected genes. (**E**) Number of commonly and differentially upregulated (top) or downregulated (bottom) genes between U373 and KUGBM8 cells and their IR-Surv cell pairs. (**F**) Commonly downregulated gene sets between U373 and KUGBM8 cell pairs. (**G**) Representative enrichment plots of "Hallmark_Hypoxia" gene sets for U373 and KUGBM8 cells.

To examine the differences in gene networks and pathways between parental and IR-Surv populations, we performed Gene Set Enrichment Analysis (GSEA) over 22,000 identified pathways from different datasets. Pathways such as DNA Repair and double-stranded break repair were upregulated in U373 and KUGBM8 IR-Surv populations. This is not surprising, as surviving long-term exposure to ionizing radiation partly depends on adaptive mechanisms of DNA damage response and repair (Figure 3B) [31]. Focusing on two of the activated pathways, GOBP Regulation of DNA Repair and Reactome DNA DSB Repair,

we observed that the majority of the genes were upregulated in IR-Surv cells (Figure 3C,D, Supplementary Table S1), suggesting IR-Surv cells rewire DNA damage recognition, response, and repair pathways to adapt to extreme IR exposure, in accordance with previous reports [32]. We then focused on the common DEGs in the IR-Surv populations of the two independent cell lines. Notably, there were 101 upregulated and 318 downregulated common genes (Figure 3E). In the GSEA analysis, the common upregulated gene sets were not highly significant (with the FDR < 0.05 cut-off); however, the common downregulated gene sets identified Hypoxia-related pathways very significantly (Figure 3F,G, Supplementary Figure S2D–G). When the significantly common downregulated genes were analyzed individually in Enrichr platform using MSigDB 2021 [33–35], "Hypoxia" was again the most significantly altered gene signature (Supplementary Figure S3). In both U373 and KUGBM8 IR-Surv populations, hypoxia-related pathways were the only commonly downregulated pathways, suggesting that cells adopt a less hypoxic signature upon IR exposure as a survival mechanism.

Besides commonalities, cell line–specific DEGs were in abundance in IR-Surv cells. Accordingly, there were 442 upregulated and 485 downregulated unique genes in U373$^{60\ Gy}$ cells, and there were 2040 upregulated and 2835 downregulated unique genes in KUGBM8$^{40\ Gy}$ cells (Figure 3E), hinting to cell line–specific adaptive mechanisms for IR survival. When GSEA analyses were conducted to identify cell line–specific changes, by excluding commonly altered pathways, we observed that the majorly altered gene sets in U373$^{60\ Gy}$ cells belonged to "interferon response genes", "STAT3 targets", and infection-related pathways (Supplementary Figure S4A). In KUGBM8 cells, the number of significantly altered pathways were higher (with FDR < 0.05 cut-off). Upregulated pathways included cell cycle-related gene sets, such as "Hallmark_G2M_Chekpoint", "Hallmark_E2F_Targets", and "YO_Myc_Targets_Up". In contrast, most downregulated gene sets were extracellular matrix (ECM)-related, such as "Reactome_Collagen_Degradation", "GOCC_Collagen_containing_ECM", and "GOBP_ECM_Disassembly" among others (Supplementary Figure S4B). Together, these results from transcriptomic analysis suggest that surviving through IR might lead to several different adaptive gene expression changes specific to cell types involved and provide insights into the mechanisms for IR survival and tumor recurrence.

2.3. IR-Surv Cells Have Higher DNA Repair Capacity

The overarching goal of radiotherapy is to generate DNA damage, causing genomic instability and leading to the death of tumor cells. Indeed, one major mechanism of survival from radiotherapy is through alteration of DNA damage response and repair [13]. To this end, we examined the generation and repair of DNA double-stranded breaks induced by ionizing radiation by staining for (γH2AX) and Tumor suppressor p53-binding protein 1 (53BP1). After a single dose of 4 Gy irradiation of U373 and U373$^{60\ Gy}$, presence and clearance γH2AX or 53BP1 levels were examined at 1 h and 6 h (Figure 4A). We observed that 4 Gy IR exposure increased 53BP1-positive foci in both U373 and U373$^{60\ Gy}$ cells. The foci number decreased to approximately 40% in U373 cells and to around 25% in U373$^{60\ Gy}$ at 6 h (Figure 4B), indicating a different level of regulation of DBS repair by 53BP1 in IR-Surv cells. As an indicator of DNA DSB burden of cells, 1 h after IR treatment, both U373 and U373$^{60\ Gy}$ cells had elevated γH2AX-positive foci at comparable levels (Figure 4C). Basal levels of γH2AX foci were higher in U373$^{60\ Gy}$, plausibly due to the prolonged IR exposure from which the cells survived despite DNA damage (Supplementary Figure S4C). After 6 h, foci number did not change in U373 cells, but the γH2AX number significantly decreased in U373$^{60\ Gy}$ cells (Figure 4C), suggesting that IR-Surv populations had altered DNA DSB recognition and repair machinery and faster DSB break repair [36]. Furthermore, gene expression levels of several DNA damage response elements, such as *ATM*, *ATR*, *CHK1*, *Rad51*, and genes associated with Mismatch repair (MMR) were upregulated in U373$^{60\ Gy}$ IR-Surv cells (Figure 4D). This gene expression signature was not observed in KUGBM8 or other glioblastoma cell lines that were utilized to generate clinically relevant IR-Surv

models (Supplementary Figure S4D). Expression of O6-Methylguanosine methyltransferase-*MGMT*, an important prognostic marker for glioblastoma, was upregulated both at gene and protein levels in U373$^{60\ Gy}$ cells, but not in KUGBM8$^{40\ Gy}$ cells (Figure 4D,E). The protein levels of activated (phosphorylated) forms of Chk1 and Chk2, γH2AX, and Rad51 were all upregulated U373$^{60\ Gy}$ cells. However, activated or basal Atm and Atr kinase expression levels were lower in U373$^{60\ Gy}$ cells. Among MMR proteins, upregulation of Msh3 and Msh6 were observed in U373$^{60\ Gy}$ cells (Figure 4E). While some changes in protein levels were consistent with RNA-seq and qRT-PCR results, such as the expression of *MGMT*, *H2AX*, *Rad51*, *MSH3*, and *MSH6*, some changes were not directly correlated. However, together with the increased phosphorylated (active) protein levels of Atm, Atr, Chk1, and Chk2, our results highlighted an overall activated DDR state in IR-Surv cells.

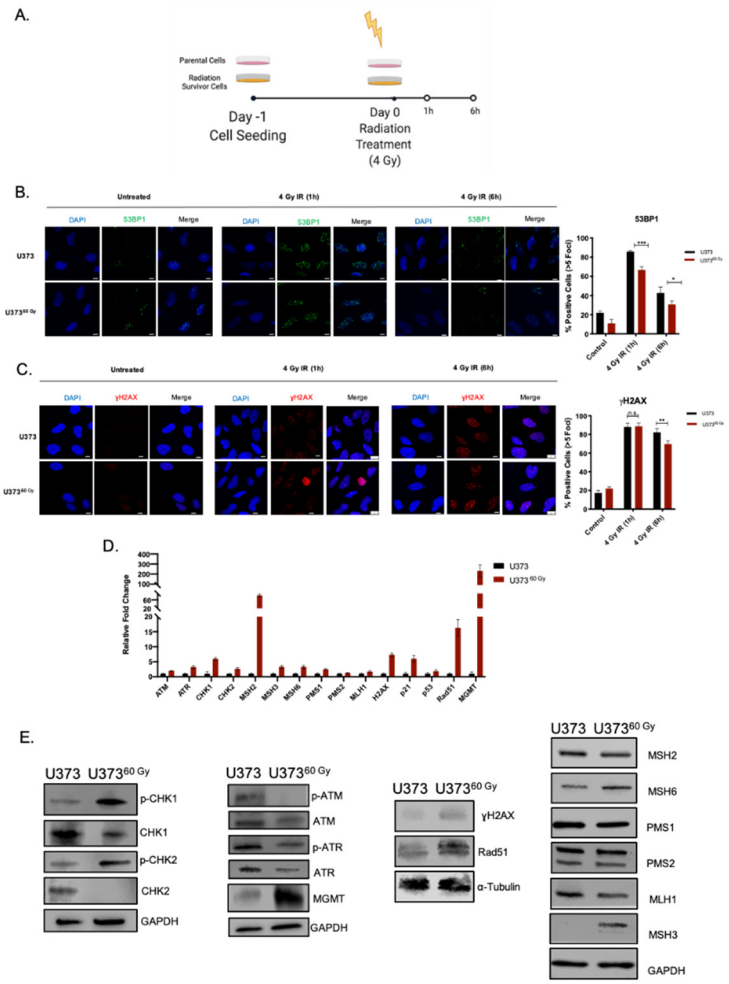

Figure 4. IR-Surv cells have higher DNA repair capacity. (**A**) Experimental setup for immunofluorescence staining for capturing DNA damage and repair (generated by Biorender.com). (**B**,**C**) Representative fluorescent images of labelled 53BP1 and γH2AX foci after 1 and 6 h of 4 Gy IR exposure of U373 and U373$^{60\ Gy}$ (Scale bar: 10 µm) (Blue: DAPI, Green: 53BP1, Red: γH2AX). (**D**) qRT-PCR results showing expression levels of different DNA damage response and repair elements. (**E**) Changes in protein levels of DNA damage response and repair elements. (ns denote not significant, for *p*-values, *, **, *** denote $p < 0.05$, $p < 0.01$, $p < 0.001$, respectively, two-way ANOVA).

DNA damage response and repair pathways are among the most targeted pathways for therapeutic purposes in cancer. Inhibition of central regulators of DDR, such as Atm, Atr, Chk1, and Chk2 is considered a prime therapeutic approach in chemo- or radiosensitization studies [37–39]. Based on our observations with IR-Surv cells, which activated DDR to adapt to long-term IR, we interrogated whether their inhibition would sensitize IR-Surv cells to

irradiation. We selected five DDR-related kinase inhibitors (DDRi) (AZD7762, AZD6738, KU55933, BML-277, and LY2603618) targeting Atm, Atr, Chk1, or Chk2 (Figure 5A). U373 and U373$^{60\ Gy}$ both responded to DDRi in a dose-dependent manner (Figure 5A,B). Further, 1 μM DDRi radiosensitized both U373 and U373$^{60\ Gy}$ cells, but the degrees of sensitization were different between them, when examined with short-term (7 day) viability assays (Figure 5C). In addition, we tested the effect of 1 μM DDRi and IR combination treatment on a long-term (14-day long) clonogenic assay. Accordingly, U373$^{60\ Gy}$ cells were slightly less responsive to KU55933 (Atm inhibitor) individual treatment, consistent with our initial findings. Combination treatment of DDRi and single-dose 4 Gy IR were very effective on both U373 and U373$^{60\ Gy}$ cells (Figure 3D,E). These results suggest IR-Surv cells with increased DNA damage response activity can be sensitized to IR treatment using DDR inhibitors.

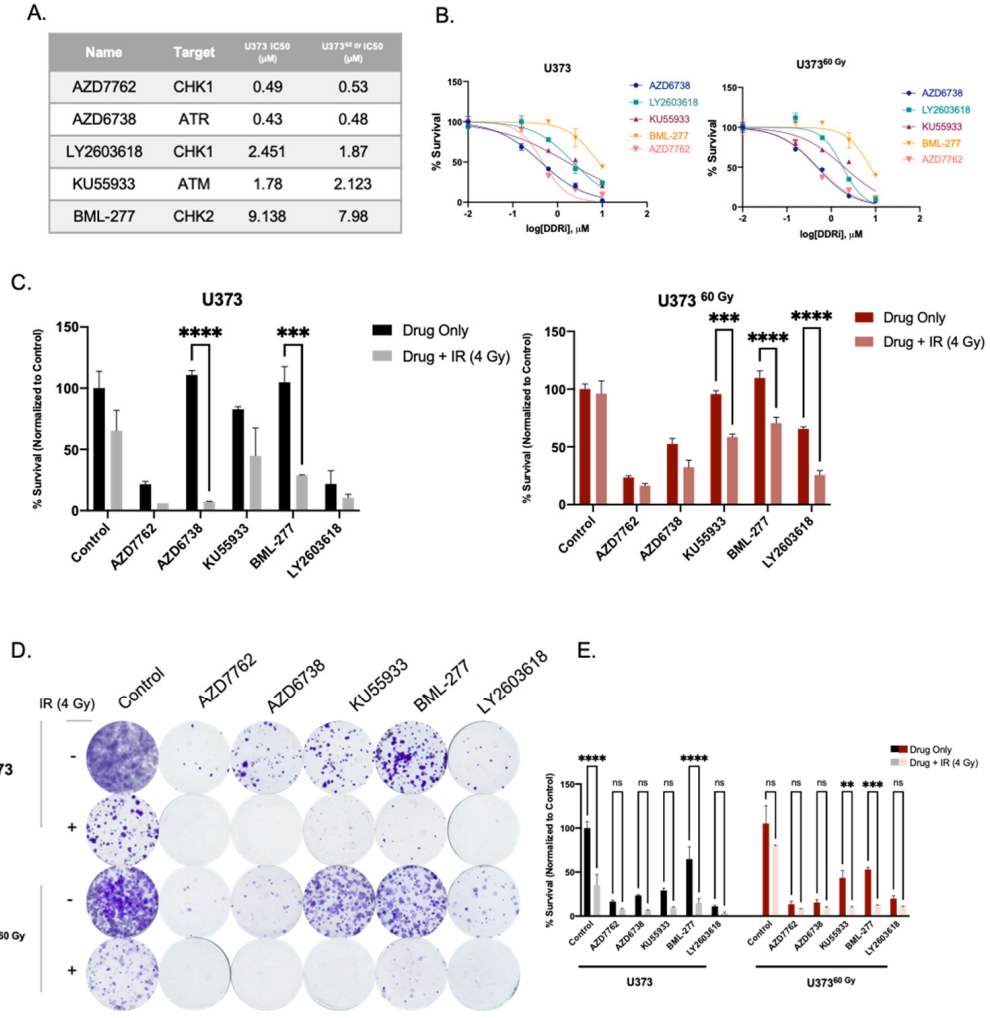

Name	Target	U373 IC50 (μM)	U373$^{60\ Gy}$ IC50 (μM)
AZD7762	CHK1	0.49	0.53
AZD6738	ATR	0.43	0.48
LY2603618	CHK1	2.451	1.87
KU55933	ATM	1.78	2.123
BML-277	CHK2	9.138	7.98

Figure 5. Inhibition of DDR-related kinases radiosensitizes U373 and U373$^{60\ Gy}$ cells. (**A**) List of inhibitors used and IC50 values of U373 and U373$^{60\ Gy}$ cells. (**B**) Dose-response curves of inhibitors of DDR-related kinases, as viability measurements 3 days after drug treatment. (**C**) Cell viability results 7 days after treatment with DDRi + IR combination on U373 and U373$^{60\ Gy}$ cells. (**D**) Representative images of clonogenic assay of combination treatment of DDRi and single-dose 4 Gy radiation on U373 and U373$^{60\ Gy}$ cells, 14 days after treatment. (**E**) Quantification of colony numbers of DDRi + IR combination treatments. (ns denote not significant, for *p*-values, **, ***, and **** denote $p < 0.01$, $p < 0.001$, and $p < 0.0001$, respectively, two-way ANOVA).

2.4. IR-Surv Cells Have Lower Hypoxic State and Exhibit Poor Response to DDR Inhibition under Further Hypoxia

As hypoxia was identified as the top downregulated pathway from our transcriptomic analysis, we investigated the behavior of IR-Surv cells by exposing them to hypoxic conditions. For this, we examined three conditions, control (normoxia), acute hypoxia (applied for 1 day) and chronic hypoxia (applied for 4 days) (Figure 6A). As a mimic for irradiation, we used DSB-causing drug Bleomycin [40] and investigated the activation of H2AX under normoxic and hypoxic conditions upon 2 h of Bleomycin treatment. Accordingly, under normoxic conditions, Bleomycin increased γH2AX activation in both U373 and U373$^{60\ Gy}$ cells significantly. The γH2AX activation levels were similar under hypoxia in U373 cells. However, U373$^{60\ Gy}$ cells exhibited slightly less γH2AX activation under hypoxic conditions, suggesting a different mode of adaptation to DNA damage and repair (Figure 6B). These adaptations have possibly affected cell cycle progression. Chronic hypoxia did not alter cell cycle distribution of U373$^{60\ Gy}$, only affecting U373 cells through G2/M arrest (Figure 6C). Downregulated response to hypoxia was also observed at gene expression level. Upon hypoxia, the extent of vascular endothelial growth factor *(VEGF)* upregulation, which can be considered a biomarker for hypoxia [41], was not the same in IR-Surv cells compared to parental cells. Specifically, upon hypoxia treatment, the *VEGF* induction was more than 20-fold in U373 parental cells, but it was less than 10-fold in U373$^{60\ Gy}$ IR-Surv cells. In addition, *CHK1* upregulation in U373$^{60\ Gy}$ cells was not observed to the same extent as in parental U373 cells (Figure 6D). To test whether the cells' response to DDRi would be altered under hypoxic conditions, we treated U373 and U373$^{60\ Gy}$ with low-dose (200 nM) Chk1 inhibitors, AZD7762 and LY2603618. To highlight their effects on cell viability, we applied 200 nM of both AZD7762 and LY603618 under normoxic and hypoxic conditions to both U373 and U373$^{60\ Gy}$ cells. While 4 days of Chk1i treatment was very effective on U373 cells, it became more effective under hypoxic conditions. However, similar cell viability was observed for U373$^{60\ Gy}$ cells under both normoxic and hypoxic conditions (Figure 6E). To test whether this phenotype is temporary or exclusive to short-term hypoxia, we performed a 14-day clonogenic assay in hypoxic conditions (Figure 6F). After Chk1i treatment, cells were incubated in a hypoxic incubator for 14 days. Clonogenic assay results revealed that U373$^{60\ Gy}$ cells were far less sensitive to Chk1i-hypoxia combination treatment than U373 cells (Figure 6G). Thus, IR-Surv cells exhibit resistance to Chk1 inhibition, and the sensitization can be achieved through IR combination, but not to sufficient degrees in hypoxic conditions.

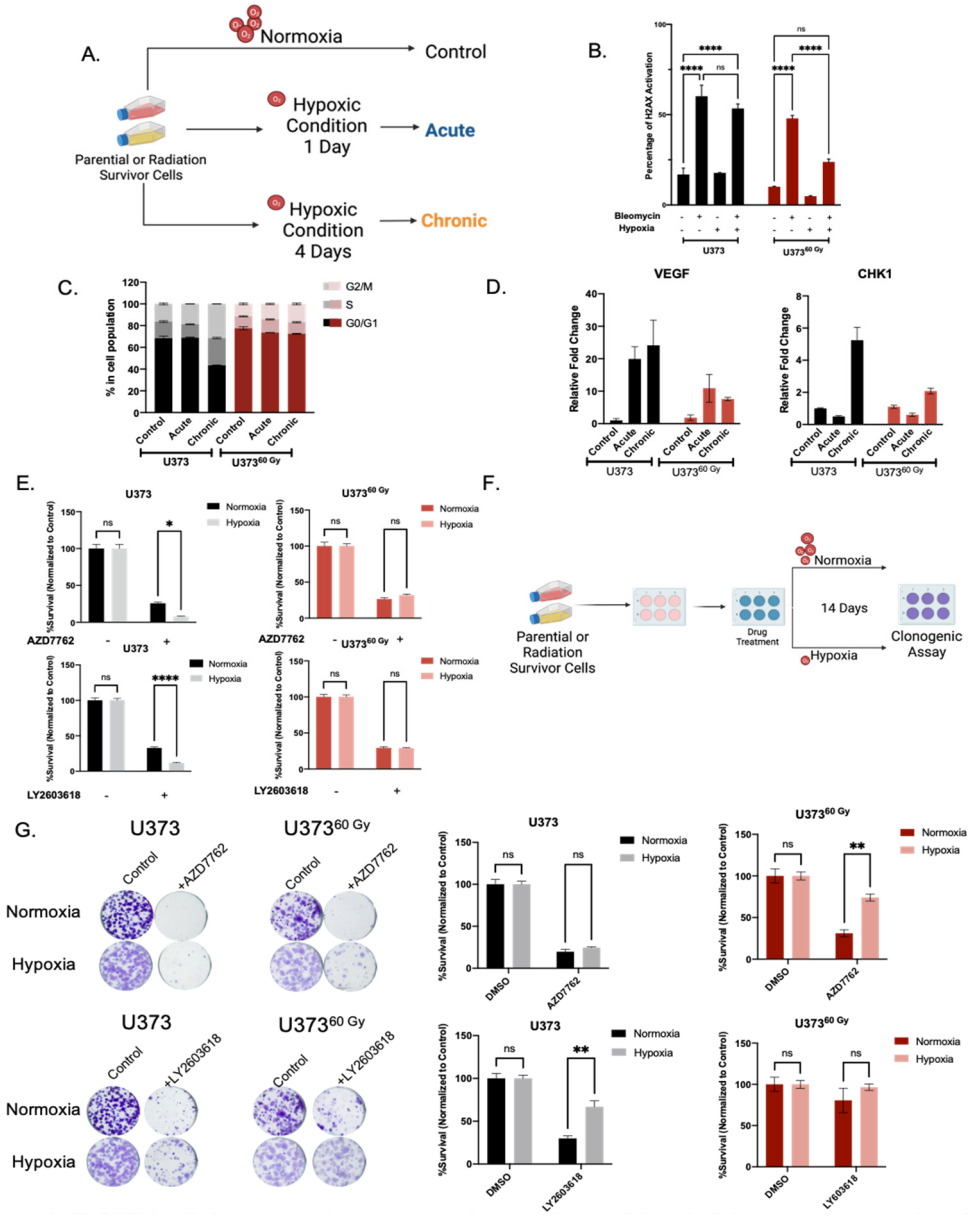

Figure 6. IR-Surv cells have poor DDRi response in hypoxic conditions. (**A**) Schematic representation of experimental flow in hypoxic conditions (generated by Biorender.com). (**B**) Assessment of H2AX activation in combination treatment of hypoxia and Bleomycin. (**C**) Cell Cycle distribution of naïve and IR-Surv cells in normoxia and hypoxia. (**D**) Gene expression levels of *CHK1* and *VEGF* upon culturing in acute and chronic hypoxia. (**E**) Cell viability differences upon treatment of CHK1 inhibitor AZD7762 and LY2603618 in normoxia and hypoxia, treatments were performed for 7 days. (**F**) Schematic representation of experimental setup for colony formation assay in long-term hypoxia. (**G**) Representative clonogenic assay images and quantification of U373 and U373$^{60\,Gy}$ cells upon treatment of CHK1 inhibitor AZD7762 and LY2603618 in normoxia and hypoxia, for 14 days. (ns denote not significant, for *p*-values, *, ** and **** denote $p < 0.05$, $p < 0.01$, $p < 0.0001$, respectively, two-way ANOVA).

3. Discussion

As high proliferation and infiltration capacity and the ability to adapt and develop resistance to therapies are significant hallmarks of the glioblastomas [42], the main treatment options of surgery, chemotherapy, and radiotherapy are not enough for cure. Despite the refined RT regimens and TMZ administration, recurrence occurs mostly in central

high dose radiotherapy field within 90% of patients due to intrinsic or acquired therapy resistance of tumor cells [5,43–45]. Therefore, understanding the molecular mechanisms behind this adaptive persistence is of utmost priority to design effective therapeutic strategies. In this study, we employed a clinically relevant radiotherapy regimen to investigate the phenotypic alterations of surviving glioblastoma cells to recapitulate the early stages of recurrence and demonstrated that IR-Surv cells had increased DNA damage repair capacity and reduced response to hypoxia and documented for the first time in literature the downregulation of hypoxic signature as well as the lower induction of hypoxia target genes, through functional assays and transcriptomic analysis.

By utilizing DNA damage response–related kinases, we showed that IR-Surv cells have a slight resistance to DNA damage response–related kinase inhibition, but these cells can be sufficiently eradicated by using inhibitors combined with single-dose IR exposure. Furthermore, we showed that both parental and IR-Surv cells reclaim resistance to Chk1 inhibition in hypoxic conditions. Together, our results suggest that IR-Surv cells may become more resistant to DDR inhibition in long-term hypoxic conditions (Figure 7), which provides insight into the future design of effective combinatorial radiotherapy strategies.

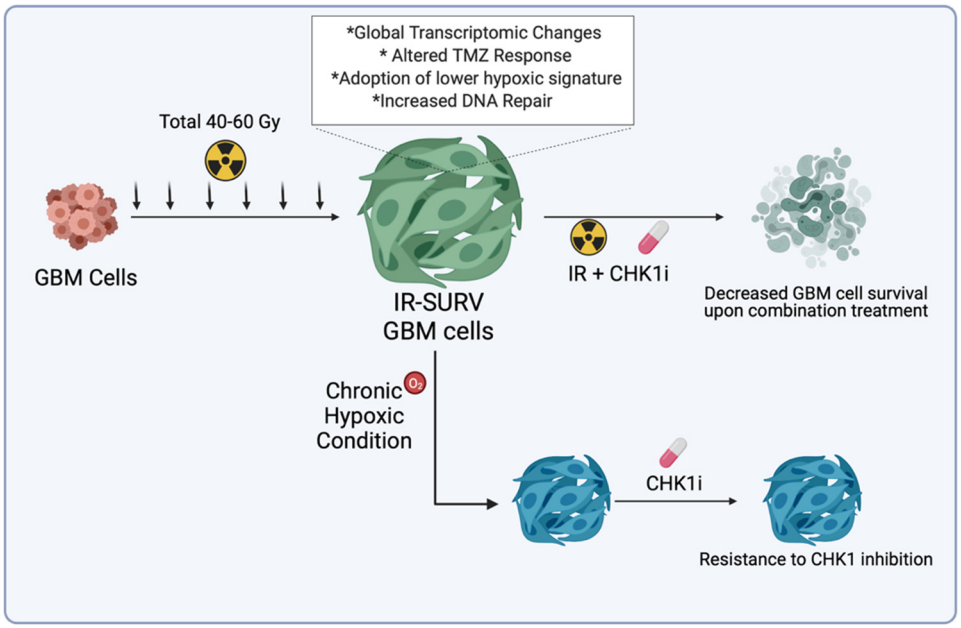

Figure 7. Graphical abstract of the study.

The radiation response and mechanisms of radioresistance are extensively studied in different cancer types, both primary and recurrent models. The model we exploit mimics the radiotherapy schedules applied to patients, which was previously used in few studies [46,47]. In the generation of radiation-survivor cell lines, we assured to remain faithful to the "Clinically Relevant Radioresistant (CRR) cell line" notion [29]. CRR concept in the generation of radioresistant cancer model is based on conventional fractional RT, exposure to 2 Gy IR once a day for more than a month. The cells were exposed to 2 Gy IR/day for five days; the fraction between two treatments was two days. In those fractioned days, cells were passaged along with parental cells to ensure cells were not under stress besides radiation therapy. This way, we succeeded in generating age-matched parental/irradiation-survivor (IR-Surv) cell line pairs. To examine the survival capacities of glioblastoma cell lines with different genetic landscapes, we utilized one primary cell line generated in our laboratory and three established cell lines [48]. However, the endurance levels of cell lines to total IR treatment were variable. The highest dose exposure was achieved by U373 cells (60 Gy), followed by KUGBM8 (40 Gy) and T98G and LN229 cells (30 Gy). The diversity of endurance of the cells may depend on various factors yet to be discovered. From the analysis of common mutations in glioblastoma, *PTEN* and *p53*

status could be among indicators of radiation persistence [49]. In the case of *PTEN*, where KUGBM8 and LN229 are wild-type, T98G cells have missense mutation. In contrast, U373 have null mutation of *PTEN*, correlating our observed radiation-survivor phenotype with different studies suggesting *PTEN* loss or mutation leading to radioresistance [50]. Except for KUGBM8 cells, all the cells used in the study were *p53* mutant. Like most glioblastoma tumors and established cell lines, radiation response depends not solely on one gene or a pathway but on various components of tumor progression [48,50].

As a representative model, we chose one established cell line and one primary cell line to investigate irradiation-induced alterations. Although U373$^{60\ Gy}$ and KUGBM8$^{40\ Gy}$ share common characteristics such as increased ratio of multinucleated cells and retained colony formation abilities after secondary IR exposure, they exhibit different phenotypes and therapy responses. We have not observed cell cycle arrest at the G1 phase in KUGBM8$^{40\ Gy}$ cells, which is reported as an indicator for radioresistance [38]. Cells may have undergone senescence after irradiation as defense mechanism, in consistency with different reports [51]. In addition, response to TMZ and adjuvant TMZ + IR differed between U373$^{60\ Gy}$ and KUGBM8$^{40\ Gy}$ cells, very likely due to differential MGMT expression levels of these IR-Surv cells. Indeed, according to our transcriptomic analysis, *MGMT* expression was upregulated in U373$^{60\ Gy}$ cells (LFC = 5.26) but downregulated in KUGBM8$^{40\ Gy}$ (LFC = −1.78). In consistent with high MGMT expression being related to poor response to TMZ [52], IR-Surv cells that upregulated MGMT displayed collateral resistance to TMZ. This suggests that some tumors may respond to TMZ when they are in a naïve state prior to IR treatment; however, prolonged IR treatment may cause the survivor tumor cells to exhibit cross-resistance to TMZ, making the chance of recurrence higher.

Our RNA sequencing analyses highlight several differentially expressed pathways in IR-Surv cells. While some of these pathways were shared between two cell lines, some were cell line–specific. For example, in U373 IR-Surv cells, interferon responsive gene networks were altered. However, in KUGBM8 IR-Surv cells, major effects were observed in ECM-related pathways, suggesting possible explanations for the phenotypic differences in U373-derived and KUGBM8-derived IR-Surv cells. It will be of future interest to decipher the relation between these pathways and IR response in our paired cell line models. Despite U373$^{60\ Gy}$ and KUGBM8$^{40\ Gy}$ exhibiting differences in functional assays and gene networks, they also shared few commonly altered pathways. As the overarching goal of radiotherapy is to generate DNA damage directly or indirectly [31,53], our results stand in parallel that IR-Surv cells show notable alterations in DNA damage response and repair pathways. With increased genomic instability, IR-Surv cells alter DNA repair machinery to survive and adapt to constant exposure to IR via increased expression of DNA damage response and repair-related proteins. This adaptation partly relies on increased DNA repair capacity. Radiation-exposed cells also survive with a higher burden of genomic instability, which is not elucidated in our study but prompts future work [54,55]. Our observations suggest that U373$^{60\ Gy}$ cells have a higher burden of DNA damage, yet upon further IR-exposure, they have higher DNA damage clearance and repair capacity than their naïve pair. We utilized a panel of inhibitors targeting DNA damage response–related kinases for radiosensitization. These DDRi inhibitors were studied in different cancer types in various conditions [39,56,57]. Our study showed that individual DDRi treatments were not sufficient for eradication of IR-Surv cells, suggesting that increased DNA repair capacity compensates for inhibition of these kinases.

Ataxia-Telangiectasia Mutated (Atm) kinase is activated explicitly upon DSB generation, which activates downstream effector kinases Checkpoint Kinase 1 (Chk1) and Checkpoint Kinase 2 (Chk2) [58]. The inhibitors of Atm, Chk1, and Chk2 kinases are extensively studied, combined with chemotherapeutic drugs and radiotherapy [20,59,60], even though multiple clinical trials are currently proceeding. As involved in regulating DDR and cell cycle checkpoints, Chk1 is among the ideal targets for radiosensitization [61,62]. Our study is consistent with radiosensitization studies in the context of Chk1 function, as radiation-mediated Chk1 activation can be exploited for radiosensitization of IR-Surv cells.

Indeed, Chk1 activation, as gauged by its gene expression and phosphorylated protein levels in IR-Surv cells, was among the most prominent changes observed in our IR-Surv cells. Therefore, it may be plausible to design therapies with Chk1 inhibitors for recurrent tumors that have high levels of activated Chk1. All in all, there is a great need for the development of new therapeutic strategies with new-generation DDR inhibitors and radiotherapy with lower cytotoxicity and improved efficacy. While several DDR inhibitors offer great promise for future clinical applications, some have failed in early stages of clinical trials. For example, a phase I trial of Chk1 inhibitor AZD7762 with irinotecan in glioblastoma was stopped because of toxicity reports (NCT00473616). To overcome the hurdles of toxicity due to high-dose drug administration, recently, new suggestions have been made en route to design effective DDRi-based combination therapies. For example, the sequence of drug administration has been suggested as an important factor to consider, as naïve tumor cells do not contain any DNA damage and do not become dependent on checkpoint kinases for their survival [37,42]. However, in our study, we show that IR-Surv tumor cells that are derived from naïve cells indeed become very adaptive to increased DNA damage and show dependency on several DDR molecules. Therefore, using inhibitors of DDR, specifically in our case, Chk1i, along with radiotherapy, might offer success in the clinic as the tumors have already completed an adaptation. This would allow for using lower doses of inhibitors and reducing the toxicity associated with drug administration. Our study might serve as a treatment model combining a low dose of DDRi and radiotherapy in both naïve and IR-Surv cell populations.

Therapy resistance of the tumors does not solely depend on the genetic and epigenetic landscape of tumor cells but is highly influenced by the tumor microenvironment [63]. Hypoxia is one of the highly studied concepts in the field of radiobiology, associated with all six R's (Repair, Redistribution, Repopulation, Reoxygenation, Reactivation of immune response, and Radiosensitivity) [64]. Indeed, the tumor core, which is highly hypoxic, is known to be more radioresistant [65,66]. Decreased oxygenation of tumor cells makes radiotherapy ineffective as ionizing radiation fails to generate reactive oxygen species that would lead to DNA damage [67]. The opposite scenario is still not elucidated. In this study, we showed that both IR-Surv cell lines exhibit downregulation of hypoxic gene signature through transcriptomic analysis and by the lower induction of hypoxia target genes, such as *VEGF*. We showed that cells that escape from chronic radiation did so by several adaptive changes, one of which resulted in a lower hypoxia response. This might seem in contrast with the knowledge in radiobiology at first sight. However, this finding, which is based on two different IR-Surv models, may suggest that tumor cells can find a way to counteract the high pressure exerted by chronic IR and become more vulnerable at the end. IR-Surv cells' response to DDR inhibition, particularly to Chk1 inhibition, was also markedly less under hypoxia in IR-Surv cells [68], suggesting that further applications of DDRi need to take into account the hypoxic nature of tumors for best clinical translation.

Taken together, we generated useful, clinically relevant radiation survivor models that exhibit several major adaptive mechanisms. We showed that efficacy of radiotherapy not only depends on hypoxic conditions but also irradiation-escaped cells that may display resistance to hypoxia. In addition, targeting DDR kinases such as Chk1 is effective on irradiation-escaped cells but the efficacy would decrease under hypoxia. These results could provide insight into designing effective treatment strategies for recurred tumors from radiotherapy.

4. Materials and Methods

4.1. Cell Culture and Reagents

Glioblastoma cell lines U373, LN229, and T98G were available from the American Tissue Type Culture Collection (USA). KUGBM8 primary cell line was established by Dr. Filiz Şenbabaoğlu from patient samples in collaboration with Koç University Hospital Neurosurgery Department; ethical approval for KUGBM8 cell line was obtained from the Koç University Institutional Review Board (2014.079.IRB2.022) [48]. Protocol of primary

cell line generation was adapted from [69]. All parental and irradiated cell populations cells were cultured in DMEM (Gibco, Gaithersburg, MD, USA) supplemented with 10% FBS (Gibco, Gaithersburg, MD, USA) and 1% Penicillin-Streptomycin (Gibco, Gaithersburg, MD, USA). All cells were maintained at 37 °C in a humidified incubator with 5% CO_2. To achieve hypoxic conditions, cells were maintained at 37 °C in a humidified incubator with 5% CO_2 and 1% O_2. AZD7762 (Selleckchem, S1532), AZD6738 (Ceralasertib, Selleckchem, S7693), LY2603618 (Rabusertib, Selleckchem, S2626), KU55933 (Selleckchem, S1092), BML-277 (Selleckchem, S8632), Bleomycin (Selleckchem, S1214), and Temozolomide (Selleckchem, S1237) were used for drug treatment experiments.

4.2. Generation of Radiation Exposed Cell Lines

Cells were irradiated with 6MV X-Ray at a dose rate of 600 MU/min in Varan iX model linear accelerator, located at the Radiation Oncology Department of Koç University Hospital. To mimic clinically relevant standardized radiotherapy, cells were exposed to 2 Gy IR every day for 4–6 weeks. U373 cell lines were exposed to 60 Gy ionizing radiation (IR) for 6 weeks. Irradiation of T98G, LN229 cell lines were concluded at 30 Gy and KUGBM8 cell irradiation was completed after 4 weeks (40 Gy).

4.3. Cell Size and Nuclei Size Analysis

All nuclei and cell size measurements were analyzed in ImageJ. Surface area of the cell size and nuclei were measured one cell at a time and plotted according to the scale. Specifically, to measure area, freehand tool was used to outline the area-of-interest.

4.4. Clonogenic Assay

All parental and irradiated cells were seeded as 750 cells/well to 6-well plates as triplicates and exposed to single doses of ionizing radiation of 2, 4, 6, or 8 Gy for each plate and incubated for 14 days. Wells were washed with 1 ×x DPBS twice, and colonies were fixed with the ice-cold methanol treatment for 5 min. After fixation, wells were washed with 1 × DPBS twice and incubated with crystal violet for 15 min. Crystal violet was removed, and plates were washed. After the plates were dried, plates were scanned, and colony densities for each well were quantified with Adobe Photoshop CC 2019 (USA).

4.5. Cell Viability Assay

Cells were seeded as 1000 cells/well, treated with the corresponding drug on day 1 and/or exposed to 4 Gy IR treatment on day 3. On day 5, MTT solution (3 mg/mL) was added as 25 µL per well and incubated for 4 h at 37 °C. After incubation, culture medium was aspirated, 100 µL DMSO was added and dissolved. Plate reading was performed in Synergy H1 Reader (BioTek, Winooski, VT, USA) at 570 nm wavelength. Survival was described as a percentage of viable cells of each sample compared with DMSO control groups.

4.6. Cell Cycle Assay

Cells were harvested from 6-well plates, and pellets were washed with ice-cold PBS. For fixation, pellets were resuspended with cold ethanol (70%) and incubated for 30 min at 4 °C. After fixation, samples were centrifuged and washed with PBS twice, resuspended in 50 µL PBS containing RNase A (100 µL /mL) and incubated at room temperature for 15 min. Propidium Iodide (PI) (50 µL/mL) was added, and samples were incubated at room temperature for 30 min. Stained samples were analyzed by BD Accuri C6 (BD Biosciences, USA) flow cytometer and 10,000 events were recorded for each sample. For cell cycle analysis in hypoxic cells, The Muse® Cell Cycle Kit (MCH100106) was used according to the manufacturer's protocol.

4.7. H2AX Activation Assay

Cells were harvested from 6-well plates following the corresponding treatment, and H2AX activation was quantified with The Muse® H2AX Activation Dual Detection Kit (MCH200101) according to the manufacturer's protocol.

4.8. Quantitative Real-Time PCR (qRT-PCR)

To determine respective mRNA expression, parental and irradiated cell pellets were collected, and RNA isolation was performed with NucleoSpin. RNA Isolation Kit according to manufacturer's instructions (Macherey-Nagel, Düren, Germany). RNA concentrations were measured with Nanodrop. With reverse transcriptase reaction, 900 ng of cDNA was obtained using M-MLV Reverse Transcriptase (Invitrogen, MA, USA). mRNA expression levels of specific genes were detected by LightCycler. 480 SYBR Green I Master (Roche). Sequences of used primers are listed in Table S2.

4.9. Western Blotting

Cell pellets were lysed in an appropriate volume of lysis buffer (1% NP40, 150 mM NaCl, 1 mM EDTA, 50 mM Tris-HCl (pH 7.8), 1 mM NaF) containing 0.1 mM PMSF and 1X protease inhibitor cocktail (complete Protease Inhibitor Cocktail Tablets, Roche). Following 30 min of incubation in the lysis buffer, the lysates were sonicated and centrifuged (12,000 rpm, 4 °C, 15 min). Samples were denatured in 4 × SDS sample buffer at 95 °C for 5 min. For equal protein loading, Pierce™ BCA (Bicinchoninic Acid) Protein Assay (Thermo Fisher, Waltham, MA, USA) was performed, and calculations were performed accordingly. For immunoblotting, equal amounts of protein were separated by SDS-polyacrylamide gel electrophoresis and transferred onto a PVDF membrane by Trans-Blot® TurboTM RTA Mini PVDF Transfer Kit (Biorad, Philadelphia, PA, USA). Later, the membranes were blocked with 5% non-fat dry milk in TBS-T (20 mM Tris-HCl, pH 7.8, 150 mM NaCl, 0.1%, v/v Tween-20) at RT for 1 h. After blocking, the membrane was incubated with primary antibodies overnight (4 °C). The list of primary antibodies is listed in Table S3. The membrane was washed three times with TBS-T for 15 min. The corresponding appropriate horseradish peroxidase coupled secondary antibodies (Cell Signaling, 1:10,000) were incubated for 1 h, and the membrane was washed three times with TBS-T. Blots were incubated with Clarity™ Western ECL Substrate (Biorad, Philadelphia, PA, USA) and visualized using an Odyssey Scanner (LiCor Biosciences, Lincoln, NE, USA).

4.10. Immunofluorescence Staining

Cells were seeded on 24-well plates on coverslips as 20.000 cells/well. After irradiation, the media was removed, and cells were washed with PBS twice. Cells were fixed with 4% PFA for 5 min at room temperature. After PBS wash, fixed cells were treated with 0.1% Triton X-100 for 5 min and washed with PBS. Each well was treated with 250 µL SuperBlock IHC Blocking Solution (ScyTek Laboratories, Logan, UT, USA) at room temperature for 15 min. After rinsing wells with PBS, coverslips were incubated with primary antibodies overnight at 4 °C. Coverslips were washed with PBS again and incubated with respective secondary antibodies at room temperature for 1 h in the dark. The list of primary and secondary antibodies is given in Table S4. Images were taken at Zeiss Axio Imager M1 (Germany) at 40× magnification. Foci numbers were counted for each condition and normalized to untreated control groups.

4.11. RNA-Sequencing and Analysis

Total RNAs of irradiated and parental cells were isolated using Macherey-Nagel NucleoSpin® RNA Isolation Kit. Based on protocols of BGISEQ-500 platform, RNA-seq libraries were prepared. Libraries were sequenced on a BGI seq 500 platform using 20 million single-end reads per sample. For U373 and U373$^{60\ Gy}$ and KUGBM8 and KUGBM8$^{40\ Gy}$, independent 3 replicate samples were sent for sequencing. Sequenced data were converted to FASTQ files using BGISEQ-500 platform at BGI Genome Sequencing Company (Beijing,

China). FASTQ files were uploaded into Genialis Expressions Platform (Genialis, Inc., Boston, MA, USA) and analyzed. According to differential expression data, volcano plots were generated, with log2(FC) = 1 and 0.05 FDR cut-offs. Heat map representations were also used for selected gene sets to visualize differential expressions. Pathway analysis was performed with Enrichr gene list enrichment analysis tool directly linked to Genialis website. Gene Set Enrichment Analysis was performed. The RNA-seq data were deposited in NCBI's Gene Expression Omnibus (GEO), with accession number GSE199862.

4.12. Statistical Analysis

All normalizations were performed on nonradiated or untreated samples, denoted as 100% using GraphPad Prism version 9.0 (USA) and Microsoft Excel 2018. Significance analysis was performed with student's *t*-test and two-way ANOVA (n.s denote not significant, for *p*-values, *, **, ***, and **** denote $p < 0.05$, $p < 0.01$, $p < 0.001$, and $p < 0.0001$, respectively, two-tailed Student's *t*-test).

Supplementary Materials: The following supporting information can be downloaded at: https://www.mdpi.com/article/10.3390/ijms23137051/s1.

Author Contributions: Study design: T.B.-O., I.S.-E. and N.P.-D.; methodology: N.P.-D., T.B.-O., U.S., Y.B. and I.S.; data generation and analysis: N.P.-D., I.S.-E. and V.A.; data interpretation: T.B.-O., N.P.-D., V.A., I.S.-E., U.S. and Y.B. drafted the manuscript: T.B.-O., N.P.-D. and I.S.-E. All authors have read and agreed to the published version of the manuscript.

Funding: Financial support was obtained from the Scientific and Technological Research Council of Turkey (TUBITAK) 117S043 (I.S.E.). The authors gratefully acknowledge the use of services and facilities of the Koç University Research Center for Translational Medicine (KUTTAM), funded by the Presidency of Turkey, Presidency of Strategy and Budget.

Institutional Review Board Statement: Not applicable.

Informed Consent Statement: Not applicable.

Data Availability Statement: The RNA-seq data have been deposited in NCBI's Gene Expression Omnibus (GEO), with accession number GSE199862.

Acknowledgments: We thank Yakup Barkodat, Esra Serbest Erkan, Mert Topçu, and Ali İhsan Atasoy at Koç University Hospital, Department of Radiation Oncology for assisting with irradiation protocols.

Conflicts of Interest: The authors declare no conflict of interest.

References

1. Wirsching, H.G.; Galanis, E.; Weller, M. Glioblastoma. *Handb. Clin. Neurol.* **2016**, *134*, 381–397. [PubMed]
2. Stupp, R.; Mason, W.P.; van den Bent, M.J.; Weller, M.; Fisher, B.; Taphoorn, M.J.B.; Belanger, K.; Brandes, A.A.; Marosi, C.; Bogdahn, U.; et al. Radiotherapy plus concomitant and adjuvant temozolomide for glioblastoma. *N. Engl. J. Med.* **2005**, *352*, 987–996. [CrossRef] [PubMed]
3. Brandes, A.A.; Tosoni, A.; Franceschi, E.; Reni, M.; Gatta, G.; Vecht, C. Glioblastoma in adults. *Crit. Rev. Oncol. Hematol.* **2008**, *67*, 139–152. [CrossRef] [PubMed]
4. McGranahan, N.; Swanton, C. Clonal Heterogeneity and Tumor Evolution: Past, Present, and the Future. *Cell* **2017**, *168*, 613–628. [CrossRef]
5. Osuka, S.; Van Meir, E.G. Overcoming therapeutic resistance in glioblastoma: The way forward. *J. Clin. Investig.* **2017**, *127*, 415–426. [CrossRef]
6. Mannino, M.; Chalmers, A.J. Radioresistance of glioma stem cells: Intrinsic characteristic or property of the "microenvironment-stem cell unit"? *Mol. Oncol.* **2011**, *5*, 374–386. [CrossRef]
7. Shimura, T.; Noma, N.; Oikawa, T.; Ochiai, Y.; Kakuda, S.; Kuwahara, Y.; Takai, Y.; Takahashi, A.; Fukumoto, M. Activation of the AKT/cyclin D1/Cdk4 survival signaling pathway in radioresistant cancer stem cells. *Oncogenesis* **2012**, *1*, e12–e19. [CrossRef]
8. Bao, S.; Wu, Q.; McLendon, R.E.; Hao, Y.; Shi, Q.; Hjelmeland, A.B.; Dewhirst, M.W.; Bigner, D.D.; Rich, J.N. Glioma stem cells promote radioresistance by preferential activation of the DNA damage response. *Nature* **2006**, *444*, 756–760. [CrossRef]
9. Serafim, R.B.; da Silva, P.; Cardoso, C.; Di Cristofaro, L.F.M.; Netto, R.P.; de Almeida, R.; Navegante, G.; Storti, C.B.; de Sousa, J.F.; de Souza, F.C.; et al. Expression Profiling of Glioblastoma Cell Lines Reveals Novel Extracellular Matrix-Receptor Genes Correlated with the Responsiveness of Glioma Patients to Ionizing Radiation. *Front. Oncol.* **2021**, *11*, 668090. [CrossRef]

10. Cuddapah, V.A.; Robel, S.; Watkins, S.; Sontheimer, H. A neurocentric perspective on glioma invasion. *Nat. Rev. Neurosci.* **2014**, *15*, 455–465. [CrossRef]
11. Basheer, A.S.; Abas, F.; Othman, I.; Naidu, R. Role of Inflammatory Mediators, Macrophages, and Neutrophils in Glioma Maintenance and Progression: Mechanistic Understanding and Potential Therapeutic Applications. *Cancers* **2021**, *13*, 4226. [CrossRef] [PubMed]
12. Roy, K.; Wang, L.; Makrigiorgos, G.M.; Price, B.D. Methylation of the ATM promoter in glioma cells alters ionizing radiation sensitivity. *Biochem. Biophys. Res. Commun.* **2006**, *344*, 821–826. [CrossRef] [PubMed]
13. Wang, C.; Zheng, W.; Yao, D.; Chen, Q.; Zhu, L.; Zhang, J.; Pan, Y.; Zhang, J.; Shao, C. Upregulation of DNA Metabolism-Related Genes Contributes to Radioresistance of Glioblastoma. *Hum. Gene Ther. Clin. Dev.* **2019**, *30*, 74–87. [CrossRef] [PubMed]
14. Fukui, R.; Saga, R.; Matsuya, Y.; Tomita, K.; Kuwahara, Y.; Ohuchi, K.; Sato, T.; Okumura, K.; Date, H.; Fukumoto, M.; et al. Tumor radioresistance caused by radiation-induced changes of stem-like cell content and sub-lethal damage repair capability. *Sci. Rep.* **2022**, *12*, 1056. [CrossRef]
15. Ali, M.Y.; Oliva, C.R.; Noman, A.S.M.; Allen, B.G.; Goswami, P.C.; Zakharia, Y.; Monga, V.; Spitz, D.R.; Buatti, J.M.; Griguer, C.E. Radioresistance in glioblastoma and the development of radiosensitizers. *Cancers* **2020**, *12*, 2511. [CrossRef] [PubMed]
16. Gupta, K.; Burns, T.C. Radiation-induced alterations in the recurrent glioblastoma microenvironment: Therapeutic implications. *Front. Oncol.* **2018**, *8*, 503. [CrossRef]
17. Mukherjee, B.; McEllin, B.; Camacho, C.V.; Tomimatsu, N.; Sirasanagandala, S.; Nannepaga, S.; Hatanpaa, K.J.; Mickey, B.; Madden, C.; Maher, E.; et al. EGFRvIII and DNA double-strand break repair: A molecular mechanism for radioresistance in glioblastoma. *Cancer Res.* **2009**, *69*, 4252–4259. [CrossRef]
18. Carruthers, R.D.; Ahmed, S.U.; Ramachandran, S.; Strathdee, K.; Kurian, K.M.; Hedley, A.; Gomez-Roman, N.; Kalna, G.; Neilson, M.; Gilmour, L.; et al. Replication stress drives constitutive activation of the DNA damage response and radioresistance in glioblastoma stem-like cells. *Cancer Res.* **2018**, *78*, 5060–5071. [CrossRef]
19. Kim, Y.H.; Yoo, K.C.; Cui, Y.H.; Uddin, N.; Lim, E.J.; Kim, M.J.; Nam, S.Y.; Kim, I.G.; Suh, Y.; Lee, S.J. Radiation promotes malignant progression of glioma cells through HIF-1alpha stabilization. *Cancer Lett.* **2014**, *354*, 132–141. [CrossRef]
20. Huang, R.X.; Zhou, P.K. DNA damage response signaling pathways and targets for radiotherapy sensitization in cancer. *Signal Transduct. Target. Ther.* **2020**, *5*, 60. [CrossRef]
21. Chen, H.H.W.; Kuo, M.T. Improving radiotherapy in cancer treatment: Promises and challenges. *Oncotarget* **2017**, *8*, 62742–62758. [CrossRef] [PubMed]
22. Morás, A.M.; Henn, J.G.; Steffens Reinhardt, L.; Lenz, G.; Moura, D.J. Recent developments in drug delivery strategies for targeting DNA damage response in glioblastoma. *Life Sci.* **2021**, *287*, 120128. [CrossRef] [PubMed]
23. Pilié, P.G.; Tang, C.; Mills, G.B.; Yap, T.A. State-of-the-art strategies for targeting the DNA damage response in cancer. *Nat. Rev. Clin. Oncol.* **2019**, *16*, 81–104. [CrossRef] [PubMed]
24. Topkan, E.; Selek, U.; Ozdemir, Y.; Yildirim, B.A.; Guler, O.C.; Ciner, F.; Mertsoylu, H.; Tufan, K. Prognostic value of the Glasgow Prognostic Score for glioblastoma multiforme patients treated with radiotherapy and temozolomide. *J. Neurooncol.* **2018**, *139*, 411–419. [CrossRef] [PubMed]
25. Menon, H.; Ramapriyan, R.; Cushman, T.R.; Verma, V.; Kim, H.H.; Schoenhals, J.E.; Atalar, C.; Selek, U.; Chun, S.G.; Chang, J.Y.; et al. Role of radiation therapy in modulation of the tumor stroma and microenvironment. *Front. Immunol.* **2019**, *10*, 193. [CrossRef] [PubMed]
26. Topkan, E.; Kucuk, A.; Ozdemir, Y.; Mertsoylu, H.; Besen, A.A.; Sezen, D.; Bolukbasi, Y.; Pehlivan, B.; Selek, U. Systemic Inflammation Response Index Predicts Survival Outcomes in Glioblastoma Multiforme Patients Treated with Standard Stupp Protocol. *J. Immunol. Res.* **2020**, *2020*, 8628540. [CrossRef]
27. Topkan, E.; Besen, A.A.; Mertsoylu, H.; Kucuk, A.; Pehlivan, B.; Selek, U. Prognostic Value of C-Reactive Protein to Albumin Ratio in Glioblastoma Multiforme Patients Treated with Concurrent Radiotherapy and Temozolomide. *Int. J. Inflamm.* **2020**, *2020*, 6947382. [CrossRef]
28. Topkan, E.; Besen, A.A.; Ozdemir, Y.; Kucuk, A.; Mertsoylu, H.; Pehlivan, B.; Selek, U. Prognostic Value of Pretreatment Systemic Immune-Inflammation Index in Glioblastoma Multiforme Patients Undergoing Postneurosurgical Radiotherapy plus Concurrent and Adjuvant Temozolomide. *Mediat. Inflamm.* **2020**, *2020*, 4392189. [CrossRef]
29. Kuwahara, Y.; Roudkenar, M.H.; Urushihara, Y.; Saito, Y.; Tomita, K.; Roushandeh, A.M.; Sato, T.; Kurimasa, A.; Fukumoto, M. Clinically relevant radioresistant cell line: A simple model to understand cancer radioresistance. *Med. Mol. Morphol.* **2017**, *50*, 195–204. [CrossRef]
30. Franken, N.A.P.; Rodermond, H.M.; Stap, J.; Haveman, J.; van Bree, C. Clonogenic assay of cells in vitro. *Nat. Protoc.* **2006**, *1*, 2315–2319. [CrossRef]
31. Maier, P.; Hartmann, L.; Wenz, F.; Herskind, C. Cellular pathways in response to ionizing radiation and their targetability for tumor radiosensitization. *Int. J. Mol. Sci.* **2016**, *17*, 102. [CrossRef] [PubMed]
32. Hein, A.L.; Ouellette, M.M.; Yan, Y. Radiation-induced signaling pathways that promote cancer cell survival (Review). *Int. J. Oncol.* **2014**, *45*, 1813–1819. [CrossRef] [PubMed]
33. Kuleshov, M.V.; Jones, M.R.; Rouillard, A.D.; Fernandez, N.F.; Duan, Q.; Wang, Z.; Koplev, S.; Jenkins, S.L.; Jagodnik, K.M.; Lachmann, A.; et al. Enrichr: A comprehensive gene set enrichment analysis web server 2016 update. *Nucleic Acids Res.* **2016**, *44*, W90–W97. [CrossRef] [PubMed]

34. Chen, E.Y.; Tan, C.M.; Kou, Y.; Duan, Q.; Wang, Z.; Meirelles, G.V.; Clark, N.R.; Ma'ayan, A. Enrichr: Interactive and collaborative HTML5 gene list enrichment analysis tool. *BMC Bioinform.* **2013**, *14*, 128. [CrossRef]
35. Xie, Z.; Bailey, A.; Kuleshov, M.V.; Clarke, D.J.B.; Evangelista, J.E.; Jenkins, S.L.; Lachmann, A.; Wojciechowicz, M.L.; Kropiwnicki, E.; Jagodnik, K.M.; et al. Gene Set Knowledge Discovery with Enrichr. *Curr. Protoc.* **2021**, *1*, e90. [CrossRef]
36. Raleigh, D.R.; Haas-Kogan, D.A. Molecular targets and mechanisms of radiosensitization using DNA damage response pathways. *Futur. Oncol.* **2013**, *9*, 219–233. [CrossRef]
37. Elmore, K.B.; Schaff, L.R. DNA Repair Mechanisms and Therapeutic Targets in Glioma. *Curr. Oncol. Rep.* **2021**, *23*, 87. [CrossRef]
38. Dillon, M.T.; Good, J.S.; Harrington, K.J. Selective Targeting of the G2/M Cell Cycle Checkpoint to Improve the Therapeutic Index of Radiotherapy. *Clin. Oncol.* **2014**, *26*, 257–265. [CrossRef]
39. Carrassa, L.; Damia, G. DNA damage response inhibitors: Mechanisms and potential applications in cancer therapy. *Cancer Treat. Rev.* **2017**, *60*, 139–151. [CrossRef]
40. Bolzán, A.D.; Bianchi, M.S. DNA and chromosome damage induced by bleomycin in mammalian cells: An update. *Mutat. Res.-Rev. Mutat. Res.* **2018**, *775*, 51–62. [CrossRef]
41. Tirpe, A.A.; Gulei, D.; Ciortea, S.M.; Crivii, C.; Berindan-Neagoe, I. Hypoxia: Overview on hypoxia-mediated mechanisms with a focus on the role of hif genes. *Int. J. Mol. Sci.* **2019**, *20*, 6140. [CrossRef] [PubMed]
42. Mooney, J.; Bernstock, J.D.; Ilyas, A.; Ibrahim, A.; Yamashita, D.; Markert, J.M.; Nakano, I. Current Approaches and Challenges in the Molecular Therapeutic Targeting of Glioblastoma. *World Neurosurg.* **2019**, *129*, 90–100. [CrossRef] [PubMed]
43. Friedman, H.S.; Kerby, T.; Calvert, H. Temozolomide and treatment of malignant glioma. *Clin. Cancer Res.* **2000**, *6*, 2585–2597. [PubMed]
44. Taal, W.; Bromberg, J.E.C.; van den Bent, M.J. Chemotherapy in glioma. *CNS Oncol.* **2015**, *4*, 179–192. [CrossRef] [PubMed]
45. Chang, E.L.; Akyurek, S.; Avalos, T.; Rebueno, N.; Spicer, C.; Garcia, J.; Famiglietti, R.; Allen, P.K.; Chao, K.S.C.; Mahajan, A.; et al. Evaluation of Peritumoral Edema in the Delineation of Radiotherapy Clinical Target Volumes for Glioblastoma. *Int. J. Radiat. Oncol. Biol. Phys.* **2007**, *68*, 144–150. [CrossRef]
46. Gray, M.; Turnbull, A.K.; Ward, C.; Meehan, J.; Martínez-Pérez, C.; Bonello, M.; Pang, L.Y.; Langdon, S.P.; Kunkler, I.H.; Murray, A.; et al. Development and characterisation of acquired radioresistant breast cancer cell lines. *Radiat. Oncol.* **2019**, *14*, 64. [CrossRef]
47. Petragnano, F.; Pietrantoni, I.; Camero, S.; Codenotti, S.; Milazzo, L.; Vulcano, F.; MacIoce, G.; Giordani, I.; Tini, P.; Cheleschi, S.; et al. Clinically relevant radioresistant rhabdomyosarcoma cell lines: Functional, molecular and immune-related characterization. *J. Biomed. Sci.* **2020**, *27*, 90. [CrossRef]
48. Senbabaoglu, F.; Aksu, A.C.; Cingoz, A.; Seker-Polat, F.; Borklu-Yucel, E.; Solaroglu, İ.; Bagci-Onder, T. Drug Repositioning Screen on a New Primary Cell Line Identifies Potent Therapeutics for Glioblastoma. *Front. Neurosci.* **2020**, *14*, 578316. [CrossRef]
49. Ma, J.; Benitez, J.A.; Li, J.; Miki, S.; Ponte de Albuquerque, C.; Galatro, T.; Orellana, L.; Zanca, C.; Reed, R.; Boyer, A.; et al. Inhibition of Nuclear PTEN Tyrosine Phosphorylation Enhances Glioma Radiation Sensitivity through Attenuated DNA Repair. *Cancer Cell* **2019**, *35*, 504–518.e7. [CrossRef]
50. Lee, J.J.; Kim, B.C.; Park, M.J.; Lee, Y.S.; Kim, Y.N.; Lee, B.L.; Lee, J.S. PTEN status switches cell fate between premature senescence and apoptosis in glioma exposed to ionizing radiation. *Cell Death Differ.* **2011**, *18*, 666–677. [CrossRef]
51. Kim, B.M.; Hong, Y.; Lee, S.; Liu, P.; Lim, J.H.; Lee, Y.H.; Lee, T.H.; Chang, K.T.; Hong, Y. Therapeutic implications for overcoming radiation resistance in cancer therapy. *Int. J. Mol. Sci.* **2015**, *16*, 26880–26913. [CrossRef] [PubMed]
52. Lee, S.Y. Temozolomide resistance in glioblastoma multiforme. *Genes Dis.* **2016**, *3*, 198–210. [CrossRef] [PubMed]
53. Marín, A.; Martín, M.; Liñán, O.; Alvarenga, F.; López, M.; Fernández, L.; Büchser, D.; Cerezo, L. Bystander effects and radiotherapy. *Rep. Pract. Oncol. Radiother.* **2015**, *20*, 12–21. [CrossRef] [PubMed]
54. Nickoloff, J.A.; Jones, D.; Lee, S.H.; Williamson, E.A.; Hromas, R. Drugging the Cancers Addicted to DNA Repair. *J. Natl. Cancer Inst.* **2017**, *109*, djx059. [CrossRef] [PubMed]
55. Motegi, A.; Masutani, M.; Yoshioka, K.; Bessho, T. Aberrations in DNA Repair Pathways in Cancer and Therapeutic Significances. *Semin. Cancer Biol.* **2019**, *58*, 29–46. [CrossRef]
56. Squatrito, M.; Brennan, C.W.; Helmy, K.; Huse, J.T.; Petrini, J.H.; Holland, E.C. Loss of ATM/Chk2/p53 Pathway Components Accelerates Tumor Development and Contributes to Radiation Resistance in Gliomas. *Cancer Cell* **2010**, *18*, 619–629. [CrossRef]
57. Dillon, M.T.; Barker, H.E.; Pedersen, M.; Hafsi, H.; Bhide, S.A.; Newbold, K.L.; Nutting, C.M.; McLaughlin, M.; Harrington, K.J. Radiosensitization by the ATR Inhibitor AZD6738 through Generation of Acentric Micronuclei. *Mol. Cancer Ther.* **2016**, *16*, 25–34. [CrossRef]
58. Vlatkovic, T.; Veldwijk, M.R.; Giordano, F.A.; Herskind, C. Targeting Cell Cycle Checkpoint Kinases to Overcome Intrinsic Radioresistance in Brain Tumor Cells. *Cancers* **2022**, *14*, 701. [CrossRef]
59. Goldstein, M.; Kastan, M.B. The DNA Damage Response: Implications for Tumor Responses to Radiation and Chemotherapy. *Annu. Rev. Med.* **2015**, *66*, 129–143. [CrossRef]
60. van Bijsterveldt, L.; Durley, S.C.; Maughan, T.S.; Humphrey, T.C. The Challenge of Combining Chemo- and Radiotherapy with Checkpoint Kinase Inhibitors. *Clin. Cancer Res.* **2021**, *27*, 937–962. [CrossRef]
61. Qiu, Z.; Oleinick, N.L.; Zhang, J. ATR/CHK1 inhibitors and cancer therapy. *Radiother. Oncol.* **2018**, *126*, 450–464. [CrossRef] [PubMed]

62. Barker, H.E.; Patel, R.; McLaughlin, M.; Schick, U.; Zaidi, S.; Nutting, C.M.; Newbold, K.L.; Bhide, S.; Harrington, K.J. CHK1 inhibition radiosensitizes head and neck cancers to paclitaxel-based chemoradiotherapy. *Mol. Cancer Ther.* **2016**, *15*, 2042–2054. [CrossRef] [PubMed]
63. Rey, S.; Schito, L.; Koritzinsky, M.; Wouters, B.G. Molecular targeting of hypoxia in radiotherapy. *Adv. Drug Deliv. Rev.* **2017**, *109*, 45–62. [CrossRef] [PubMed]
64. Boustani, J.; Grapin, M.; Laurent, P.A.; Apetoh, L.; Mirjolet, C. The 6th R of radiobiology: Reactivation of anti-tumor immune response. *Cancers* **2019**, *11*, 860. [CrossRef]
65. Jarosz-Biej, M.; Smolarczyk, R.; Cichoń, T.; Kułach, N. Tumor Microenvironment as A "Game Changer" in Cancer Radiotherapy. *Int. J. Mol. Sci.* **2019**, *20*, 3212. [CrossRef]
66. Boulefour, W.; Rowinski, E.; Louati, S.; Sotton, S.; Wozny, A.S.; Moreno-Acosta, P.; Mery, B.; Rodriguez-Lafrasse, C.; Magne, N. A review of the role of hypoxia in radioresistance in cancer therapy. *Med. Sci. Monit.* **2021**, *27*, 1–7.
67. Moeller, B.J.; Richardson, R.A.; Dewhirst, M.W. Hypoxia and radiotherapy: Opportunities for improved outcomes in cancer treatment. *Cancer Metastasis Rev.* **2007**, *26*, 241–248. [CrossRef]
68. Hasvold, G.; Nähse-Kumpf, V.; Tkacz-Stachowska, K.; Rofstad, E.K.; Syljuåsen, R.G. The efficacy of CHK1 inhibitors is not altered by hypoxia, but is enhanced after reoxygenation. *Mol. Cancer Ther.* **2013**, *12*, 705–716. [CrossRef]
69. Xie, Y.; Bergström, T.; Jiang, Y.; Johansson, P.; Marinescu, V.D.; Lindberg, N.; Segerman, A.; Wicher, G.; Niklasson, M.; Baskaran, S.; et al. The Human Glioblastoma Cell Culture Resource: Validated Cell Models Representing All Molecular Subtypes. *EBioMedicine* **2015**, *2*, 1351–1363. [CrossRef]